Journal of Translational Medicine

RESEARCH

Open Access

Colorectal cancer cells-derived exosomal miR-188-3p promotes liver metastasis by creating a pre-metastatic niche via activation of hepatic stellate cells

Tao Li[1,2†], Taiyuan Li[1,2†], Yahang Liang[1,2†], Yuli Yuan[1,2], Yang Liu[1,2], Yao Yao[1,2] and Xiong Lei[1,2*]

Abstract

Background/Aim Metastasis is the leading cause of mortality for colorectal cancer (CRC). Cancer-derived exosomes are widely recognized as the primary catalysts behind the development of pre-metastasis niche (PMN) in distal sites. However, the exact mechanism behind this process in CRC remains elusive. This study aimed to investigate the function and mechanisms underlying the role of exosomal miR-188-3p in activating hepatic stellate cells (HSCs) to develop the PMN and promote liver metastasis.

Methods We extracted exosomes from CRC cells using ultracentrifugation. Exosomes were identified using transmission electron microscopy, nanoparticle tracking analysis, and Western blot. Exosome uptake was assessed using fluorescence tracing, exosome PKH67 staining, and real-time quantitative PCR. The effects of CRC cell-derived exosomes on HSCs migration were evaluated using Transwell migration and wound healing assays. Key differentially expressed miRNAs were screened from the GEO database, and bioinformatics prediction along with dual-luciferase reporter assays were used to identify downstream target genes of miR-188-3p. Downstream related proteins of the target genes were detected by Western blot. In vivo, the distribution of exosomes and activation of HSCs in the liver were explored by tail vein injection of exosomes into nude mice. Further, the impact of exosomal miR-188-3p on liver metastasis was investigated using a spleen injection liver metastasis model. Finally, the expression levels of miR-188-3p in exosomes from CRC patient plasma were determined by real-time quantitative PCR, and the relationship between the expression of miR-188-3p in plasma exosomes and CRC prognosis was analyzed.

Results The expression level of miR-188-3p within plasma exosomes demonstrated a statistically significant increase in CRC with liver metastasis compared to those without liver metastases. We also demonstrated the transferability of miR-188-3p from CRC cells to HSCs cells via the exosomes. Exosomal miR-188-3p plays a pivotal role in orchestrating the establishment of PMN through targeting PHLPP2 to activate HSCs before tumor metastasis. Exosomal miR-188-3p

†Tao Li, Taiyuan Li and Yahang Liang contributed equally to this work.

*Correspondence:
Xiong Lei
leixionglinty@126.com

Full list of author information is available at the end of the article

was found to actively foster in vivo metastasis of CRC. Additionally, plasma exosomal miR-188-3p potentially serves as a viable blood-based biomarker for CRLM.

Conclusion Exosomal miR-188-3p derived from CRC cells can promote liver metastasis by activating HSCs to form a PMN through targeting PHLPP2 to activate the AKT/mTOR pathway. These results offer a new perspective on the mechanisms driving CRLM.

Graphical abstract

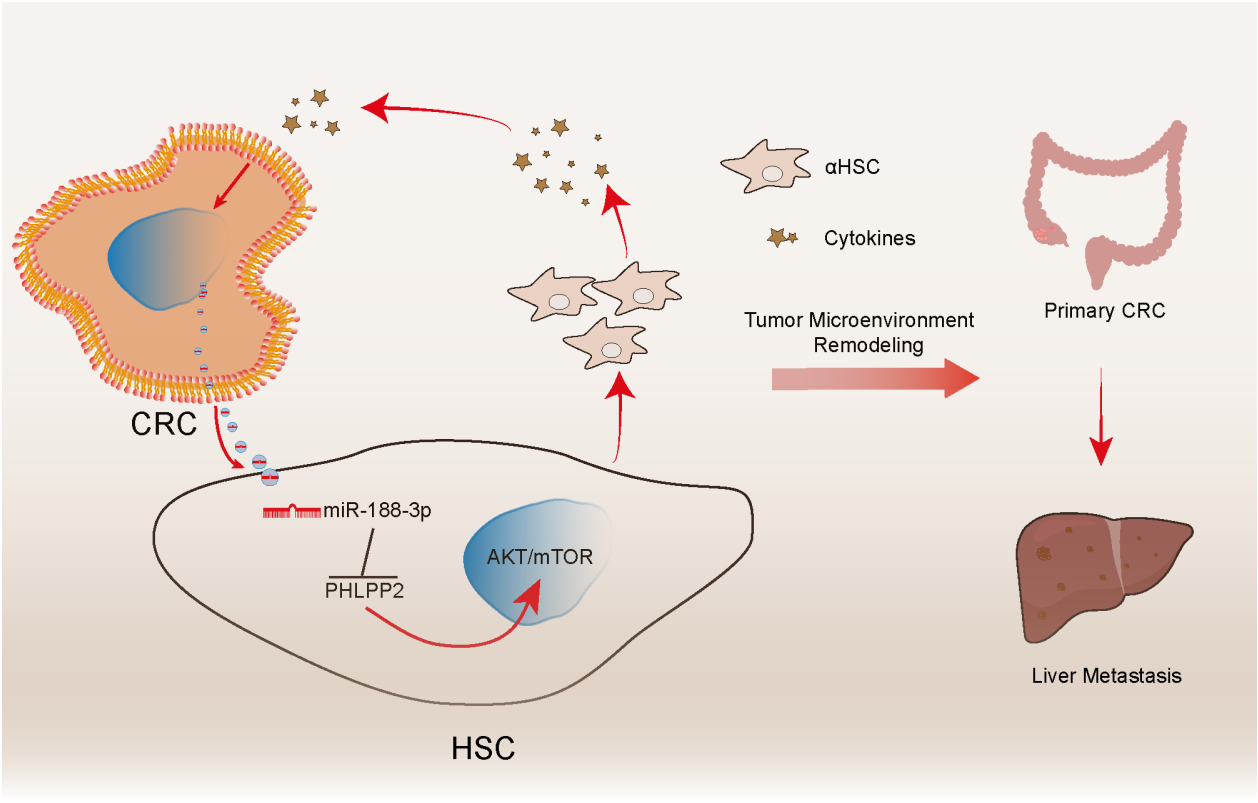

Keywords Colorectal cancer, Pre-metastatic niche, Liver metastasis, Exosome, Hepatic stellate cells

Introduction

Colorectal cancer (CRC) is a prevalent malignant tumor, ranking third in cancer incidence and second in mortality worldwide [1, 2]. Various treatment approaches like surgery, chemotherapy, radiotherapy, immunotherapy, and molecular targeted therapy have markedly increased the survival rate in patients with CRC [3]. Nevertheless, the liver is the most important target organ for CRC metastasis [4, 5], with more than half of CRC patients experience the development of liver metastases during their lifetime, ultimately leading to mortality in over two-thirds of these cases [6, 7], which posing a significant obstacle to their long-term survival. Therefore, it is essential to thoroughly investigate the pathological and molecular mechanisms behind liver metastasis and develop more effective therapeutic strategies to enhance the survival rates of CRC liver metastasis (CRLM) patients.

Numerous studies have provided insights into the pathological and molecular mechanisms that regulate the progression of primary tumors and their metastasis to distant organs [8–10]. The metastasis of CRC constitutes an intricate, multifactorial, and sequential process [11–13], however, the specific mechanism underlying each of these processes remains to be completely elucidated. Based on the "seed and soil" theory, tumor cells have the capacity to induce the formation of a supportive microenvironment in the target organ for metastasis, known as the "pre-metastatic niche" (PMN) [14]. Growing evidence underscores the importance of PMN formation, which plays a crucial role in establishing a tumor microenvironment that supports metastasis, even before disseminated tumor cells arrive and colonize the site [15–17]. During the CRLM process, CRC cells possess the ability to initiate the creation of PMN through the modification of the

liver [18], which has a pivotal influence on CRLM. However, key molecular and cellular interactions between CRC cells and the liver microenvironment, including how CRC cells specifically modify the liver to establish a PMN, are still poorly understood. Hence, investigating the mechanisms regulating the PMN formation by CRC cells emerges as a critical endeavor to enhance our comprehension of CRLM.

Hepatic stellate cells (HSCs), as the principal stromal cells in the liver, regulate the cancer progression through various mechanisms, including cytokine secretion and extracellular matrix (ECM) remodeling [19, 20]. However, whether HSCs are involved in the process of CRLM remains to be further explored. Previous studies have reported that the activation of HSCs facilitates the establishment of a PMN conducive to metastasis [21]. Meanwhile, it has been reported that the leading biological signature in cases of both primary and secondary liver cancer is characterized by the presence of α-SMA, named activated HSCs (aHSCs) [22, 23]. aHSCs with highly migratory and proliferative hallmarks are transdifferentiated from stationary hepatic stellate cells [23]. Moreover, aHSCs can impact the growth and invasion of CRC cells by participating in the remodeling and deposition of the ECM [24]. Our previous study found that activated HSCs in the PNLT were an independent predictor for CRALM recurrence following resection, indicating its role in PMN formation [25]. Therefore, a thorough investigation into the interplay between CRC cells and HSCs activation involved in PMN formation, as well as the underlying mechanisms, may pave the way for progress in preventing CRLM.

Exosomes are extracellular vesicles with a diameter of 40 ~ 160 nm, which can carry RNA and other substances, and are the communication medium among cells [26]. Among the biomolecules carried by exosomes, microRNAs (miRNAs) have garnered significant attention due to their pivotal role in gene expression regulation [27]. The miRNAs within tumor cells can be transported via exosomes to neighboring stromal cells within the tumor microenvironment, where they are internalized and subsequently lead to the "reprogramming" of pertinent target genes [28]. For instance, research has demonstrated that specific miRNAs or gene could serve as potential markers in HCC, facilitating metastasis and influencing tumor behavior [29, 30]. However, the specific miRNAs involved in CRLM and their mechanisms remain poorly understood, particularly in the activation of HSCs to create a supportive PMN, is still an understudied area of research. Based on this, it was necessary to investigate whether exosome miRNAs secreted by CRC cells can promote liver metastasis by activating HSCs to form a PMN. The present study aimed to investigate the function and mechanisms underlying the role of exosomal miR-188-3p in activating HSCs to develop the PMN and promote liver metastasis.

In this study, it was uncovered that highly metastatic CRC cells discharged exosomes rich in miR-188-3p, which played a pivotal role in driving liver metastasis by controlling the interplay between CRC cells and HSCs and reshaping the PMN. These findings have revealed a new and specific biomarker for CRLM, as well as a fresh strategy for predicting the risk of secondary liver cancer resulting from CRC.

Materials and methods

Patients and clinical specimens

From January 2012 to December 2020, a total of 214 patients diagnosed with and treated for CRC and 20 patients with CRLM were included in the study. All individuals included in this study were sourced from the First Affiliated Hospital of Nanchang University. Human blood samples were collected before tumor resection, and plasma is separated by centrifugation at 1500–2000 ×g for 10–15 min at 4 °C.while normal mucosa and paired cancer tissues, along with metastatic tissues, were gathered immediately following surgical removal. All patients provided written informed consent, and the study procedure followed the ethical principles specified in the 1975 Declaration of Helsinki. The Ethics Committee of our institution granted approval for the study protocol (Approval No. CDYFY-IACUC-202205GR010).

Cell culture

The human CRC cell lines SW480, LoVo, Caco2, HCT116 and the HSC line LX-2, were purchased from The Cell Bank of Type Culture Collection of the Chinese Academy of Sciences (Shanghai Institute of Cell Biology). All of these cells were cultured in Dulbecco's Modified Eagle Medium (DMEM) (Gibco, Grand Island, NY, USA) supplemented with 10% FBS (Gibco), glutamine, sodium pyruvate, and 1% penicillin-streptomycin. The cells were cultivated in a temperature-controlled environment at 37 °C with 5% CO2.

Exosome isolation and characterization

Exosomes were extracted from 240 mL of CRC cell supernatant and 1 mL of plasma obtained from patients. Cells were cultured in a medium supplemented with 10% exosome-depleted FBS. In brief, cell supernatants (collected after 48 h) or serum samples were subjected to sequential centrifugation at 300×g for 10 min, 2000×g for 20 min, and 10,000×g for 30 min to eliminate cellular debris. Subsequently, the supernatants were filtered using a 0.22-μm filter, followed by classical differential ultracentrifugation at 120,000×g for 70 min at 4 °C each time with an Optima XPN-100 Ultracentrifuge (Beckman Coulter, USA). Next, the exosomes were rehydrated

in 200 μL of phosphate-buffered saline (PBS), and their concentration was determined using a BCA protein assay kit (Servicebio, Wuhan, China). Transmission electron microscopy (TEM) was employed to visualize the cup-shaped morphology and membrane structure of isolated exosomes. Take 10 μl of the exosome suspension and drop it onto a copper grid, allowing it to settle for 1 min to form a precipitate. Then, use filter paper to remove the excess liquid and add 10 μl of 2% uranyl acetate solution onto the grid, allowing it to incubate for 1 min. Dry the sample at room temperature for a few minutes, then load it into the Hitachi HT7800 TEM (Hitachi High-Tech Corporation, Tokyo, Japan) and image the sample at a voltage of 80–120 kV. The NanoSight LM10 system (Malvern Instruments, UK) was used to analyze the quantity and concentration of exosomes. The exosomes were subjected to laser irradiation, their Brownian motion was recorded, and a 10-second video segment was analyzed. The expression of exosome markers CD9, TSG101, Alix, and calnexin was assessed using Western blot analysis. Details regarding the antibodies used to detect the aforementioned markers are available in Table S2 of the supplementary materials.

qRT-PCR analysis

RNA was extracted, reverse transcribed, and subjected to quantitative reverse transcription polymerase chain reaction (qRT-PCR) following previously described methods [31]. The sequences of the primers used are detailed in Table S1 of the supplemental material.

Dual luciferase reporter assay

The 3′-UTR segment of the PHLPP2 gene was amplified and cloned into vectors. For the dual luciferase reporter assay, LX-2 cells were plated in 24-well plates and treated with 40 nM of either miR-188-3p mimic or inhibitor. Transfection efficiency was evaluated using Renilla luciferase vectors. After 48 h, cells were harvested and the relative light units were measured as per the manufacturer's protocol.

Transwell assay and wound healing assay

Transwell assay was performed as described previously [31]. For wound healing assay, cells were seeded into a 6-well plate and allowed to grow to confluence. A straight scratch was made through the cell monolayer using a sterile pipette tip. The wells were then gently washed with PBS to remove detached cells and debris. Fresh medium, with or without the experimental treatment, was added to the wells. The cells were incubated under standard culture conditions (37 °C, 5% CO2). At specific time points, photographs of the scratch area were taken using a microscope. The width of the scratch was measured at different time points to assess cell migration and wound closure, with comparisons made between the initial and final scratch widths.

H&E staining

First, immerse the samples in xylene I and II for 5 min each, followed by absolute ethanol I and II for 5 min each. Next, soak the samples in 95%, 85%, and 70% ethanol for 5 min each, and finally rinse with pure water for 5 min. Stain with hematoxylin for 4 min, then rinse with tap water for 10 min. Treat with hydrochloric acid ethanol for 3 s, rinse again with tap water for 10 min, and stain with eosin for 30 s. Use absolute ethanol three times, 5 min each, to complete the dehydration process. Clear the sections by treating them with xylene I and II for 5 min each. Mount the sections with neutral resin and allow them to dry naturally, then observe and photograph under a microscope.

Animal models

The animal experimentation protocols detailed in this study underwent rigorous evaluation and received official approval from the Animal Ethics Committee at The First Affiliated Hospital of Nanchang University (No. CDYFY-IACUC-202205GR010). Eighty male BALB/c nude mice, aged 3–4 weeks and weighing 10–15 g, utilized in this study were sourced from the Zhejiang Vital River Laboratory Animal Technology Co., Ltd. and were meticulously maintained in a controlled, pathogen-free setting. Concisely, mice were initially randomly grouped, with each group consisting of 3 mice, in alignment with the experimental design's specifications. Ten μg of exosomes sourced from distinctively treated SW480, LoVo, Caco2, and HCT116 cells were suspended in 150 μl of PBS and subsequently administered via intravenous injection through the mice's tail veins. The administration of exosomes through the tail vein was repeated every 2 days over a span of 2 weeks, a procedure referred to as 'exosome education' [32]. Following exosome injection, one group of animals was immediately euthanized by cervical dislocation to procure liver specimens for frozen sectioning, while another group underwent injections of two million HCT116 cells transfected with luciferase lentivirus via the spleen and three nude mice were included in each group. Three weeks subsequent to spleen injection, the mice were examined via an in vivo image system (IVIS) (Calliper Life Sciences, Hopkinton, MA, USA). Subsequently, the mice were euthanized to extract their livers for photographic documentation and H&E staining.

Protein extraction and Western blot

Proteins from cells were extracted using RIPA lysis buffer (Servicebio, Wuhan, China) supplemented with protease and phosphatase inhibitors (Servicebio, Wuhan, China).

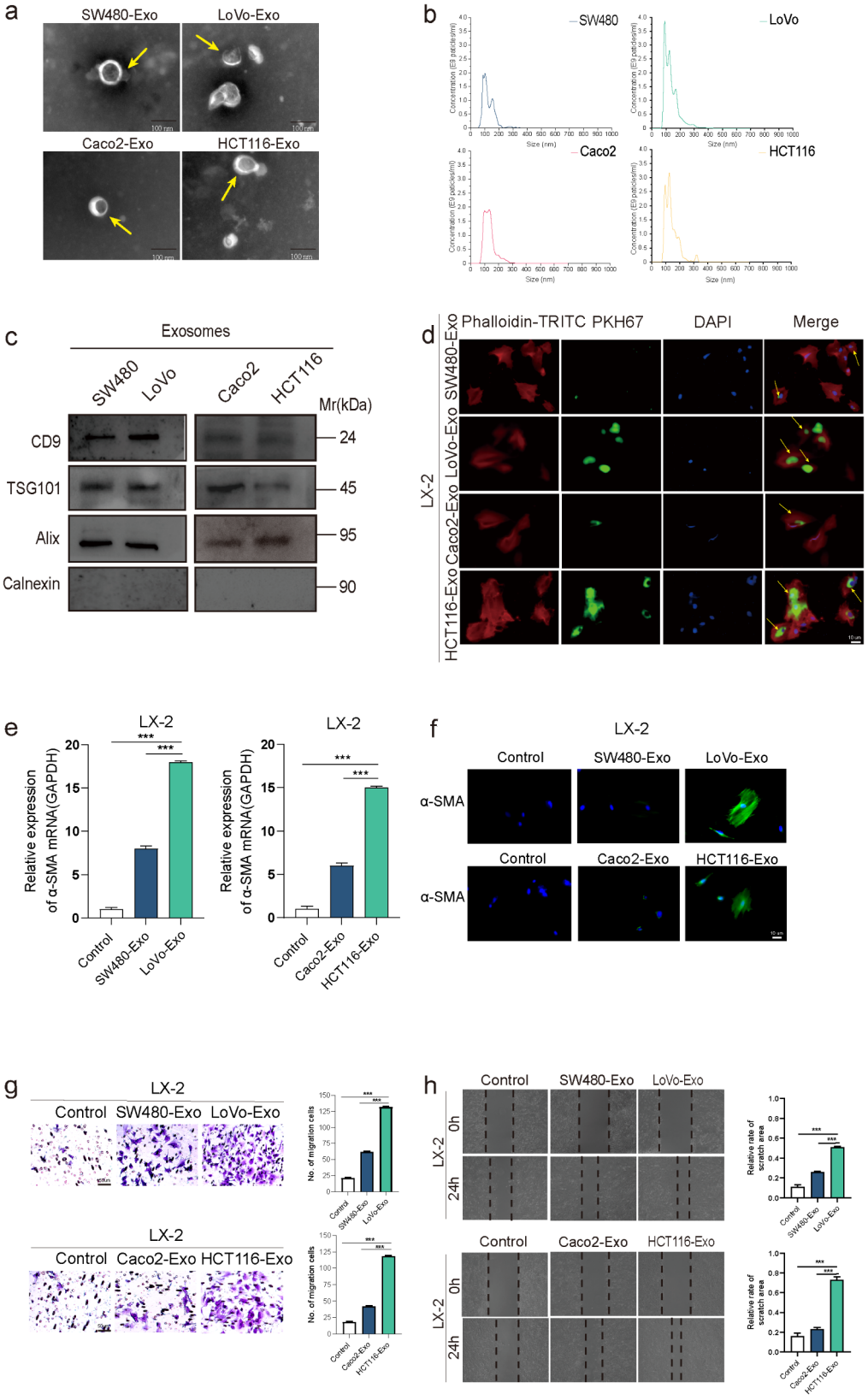

Fig. 1 (See legend on next page.)

(See figure on previous page.)

Fig. 1 High-metastatic CRC cell-derived exosomes regulate HSCs activation in vitro. (**a**) Representative images of exosomes from two groups of CRC cell lines with low and high metastasis (SW480/Caco2 and LoVo/HCT116) were captured using TEM. Scale bar = 100 nm. (**b**) Purified exosomes from four CRC cell lines were analyzed using nanoparticle tracking analysis with Nano Sight. (**c**) WB analysis of exosome markers (CD9, TSG101 and Alix) in exosomes from four CRC cell lines. (**d**) LX-2 cells were incubated with PKH67-labelled exosomes (30 μg/ml) from CRC cell lines (SW480, LoVo, Caco2, HCT116) for 24 h, and representative immunofluorescence images illustrate the delivery of PKH67-labelled CRC cell-derived exosomes (green) into Phalloidin-TRITC-labelled LX-2 cells (red); yellow arrows indicate exosomes. Scale bar = 10 μm. (**e**) The expression of the activated hepatic stellate cells (aHSCs) marker (α-SMA) in LX-2 cells incubated with exosomes derived from SW480/LoVo and Caco2/HCT116 cells, or PBS (control), was examined using qRT-PCR. (**f**) Immunofluorescence images showed the levels of α-SMA in LX-2 cells incubated with exosomes from different CRC cells, or PBS (control). Scale bar = 50 μm. **g**, **h.** Transwell and wound-healing assays were employed to assess the role of exosomes (equal quantities) derived from different CRC cells on the migratory capability of LX-2 cells. scale bar = 50 μm

The lysate was treated with SDS-PAGE protein buffer (Servicebio, Wuhan, China) and the proteins were denatured at 100 °C for 5 min. After SDS–polyacrylamide gel electrophoresis separation, the protein samples were transferred onto polyvinylidene difluoride membranes (Millipore, MA, USA). These membranes were blocked with 5% fast blocking buffer (Beyotime, Shanghai, China) for 45 min, followed by overnight incubation with primary antibodies at 4 °C. Subsequently, the membranes were immunoblotted with secondary antibodies for 2 h. Finally, protein bands were detected using Tanon's Super chemiluminescent reagent (Shanghai, China) on a ChemiDoc XRS system (Bio-Rad, CA, U.S.A.) and the grayscale of protein bands was analyzed using ImageJ software. The primary and secondary antibodies used in the Western blot are detailed in Table S2 of the supplemental material.

Immunofluorescence (IF)

LX-2 cells were seeded onto suitably dimensioned slides within 24-well plates. Following the designated pretreatments, they were fixed using a 4% paraformaldehyde solution in PBS and maintained for 10 min at ambient temperature. The livers of mice subjected to various pretreatments were harvested, embedded in optimal cutting temperature (OCT) freezing medium, and then cryosectioned into sections measuring 10 μm in thickness. These sections underwent a preliminary block using 5% goat serum, followed by an overnight incubation at 4℃ with the primary antibody α-SMA (Proteintech, Wuhan, China). Subsequently, an Alexa Fluor 488-labeled secondary antibody was applied for 1 h at 37℃. Nuclei were counterstained with DAPI. Image acquisition was performed using either fluorescence microscopy (Primo Vert iLED, Germany) or confocal microscopy (Olympus BX51, Japan). Fluorescence images were subjected to semi-quantitative analysis using Image-Pro Plus 6.0.

Statistical analysis

The statistical analyses were executed utilizing SPSS 27.0 (IBM, Chicago, IL, USA), GraphPad Prism 8.4 (GraphPad Software Inc, CA, USA), and R software (version 3.6.1). The results from more than three independent experiments are expressed as the mean ± standard deviation. Differences between groups were assessed using the student's t-test, the Mann-Whitney U test, one-way analysis of variance (ANOVA), or the chi-squared test, as appropriate. The Kaplan-Meier method and log-rank test were employed for DFS and OS. The Cox proportional hazards regression model was utilized to analyze independent predictive indicators associated with PFS and OS. P-value < 0.05 was regarded as statistically significant.

Results

High-metastatic CRC cell-derived exosomes exhibit potent HSCs activation in vitro

aHSCs have been shown to actively contribute to the progression of tumor metastasis [33]. The high expression of α-SMA, serving as the activated status of HSCs, yielded similar outcomes in CRLM tissues (FIGURE S1). Therefore, it is of utmost significance to gain a deeper comprehension of the activation of HSCs induced by tumor cells. Considering the crucial role of exosome secretion by tumors in inducing systemic alterations, it naturally raises the question of whether exosomes are involved in activating HSC. Therefore, to investigate the differential potential of HSC activated by exosomes derived from CRC cells, two pairs of CRC cell lines with distinct metastatic potentials were selected, among which LoVo and HCT116 were high-metastatic cancer cells, versus SW480 and Caco2 (FIGURE S2). First, exosomes were extracted and purified from the conditioned medium (CM) of the CRC cells using the standard ultracentrifugation method. The morphology of exosomes was observed by transmission electron microscopy (TEM), and the size distribution and number of exosomes were detected by nanoparticle tracking analyzer (NTA). TEM revealed typical cup-shaped particles with double membranes, ranging from 40 to 160 nm in diameter. Additionally, NTA indicated that exosomes from both cell lines were slightly larger than 100 nm. (FIGURE 1a, b; FIGURE S3a-d). Additionally, the CRC cell-derived exosomes was assessed by analyzing the expression of exosome markers (CD9, TSG101, and Alix) and confirming the absence of endoplasmic reticulum components (calnexin) (Fig. 1c). Furthermore, to evaluate the impact of CRC cell-derived exosomes on HSC activation, LX-2 cells were utilized as a representative HSC line. To visualize exosome delivery,

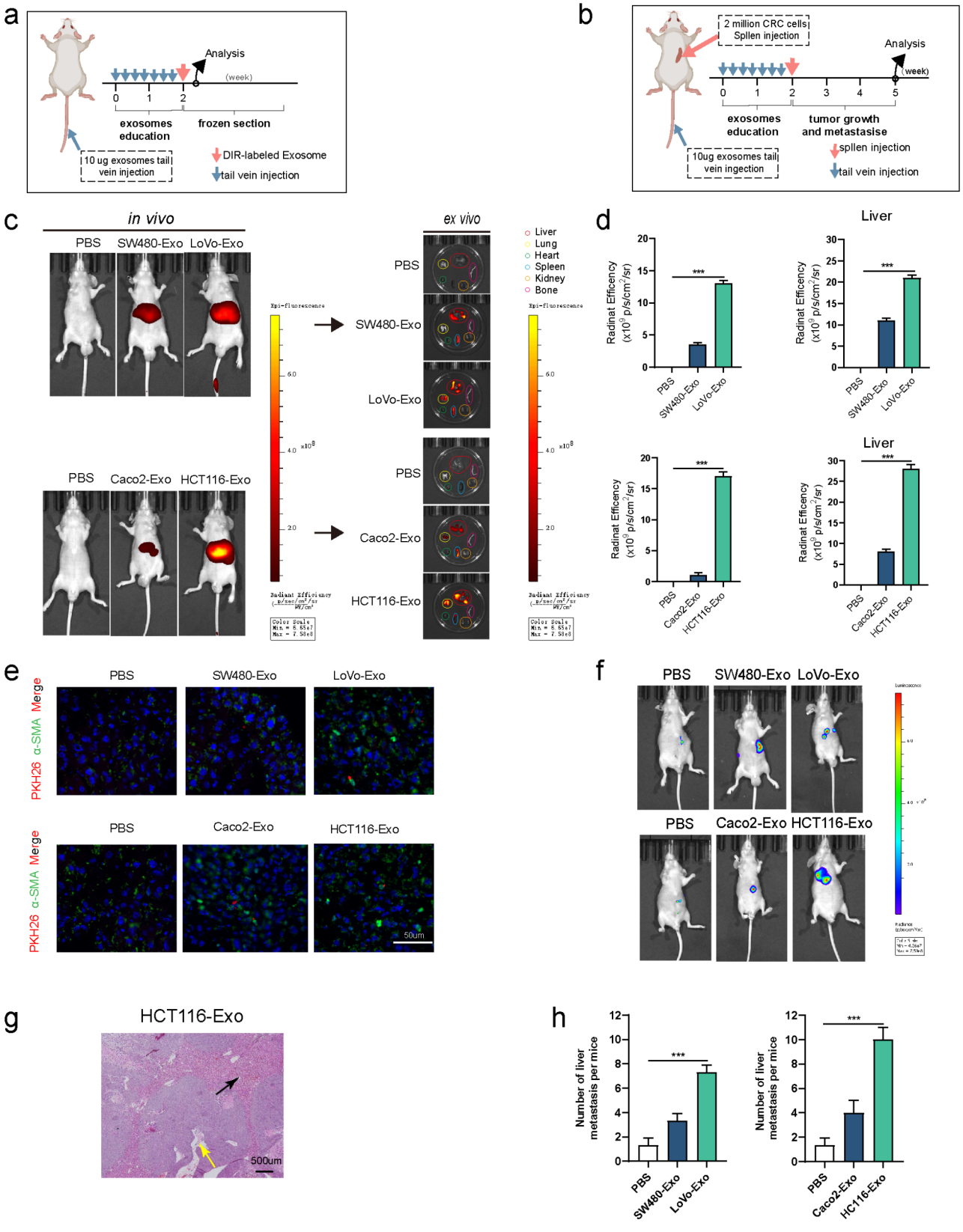

Fig. 2 (See legend on next page.)

(See figure on previous page.)

Fig. 2 High-metastatic CRC cell-derived exosomes regulate HSCs activation in CRLM progression in vivo. (**a**) Schematic representation of the establishment process of the exosome-educated animal model. (**b**) Schematic representation of the establishment process of the exosome-educated CRC liver metastases (CRLM) model. **c**, **d.** Representative in vivo imaging system (IVIS) results of mice educated with PBS, SW480, LoVo, Caco2, or HCT116 exosomes, respectively. Results of quantified values of bioluminescence imaging signals are expressed as mean ± standard deviation ($n = 3$). **e.** Representative immunofluorescence showing colocalization between exosomes and LX-2 (α-SMA) in mouse liver after tail vein injection of PKH26-labeled exosomes. Scale bar = 50 μm. **f.** Representative in vivo imaging system (IVIS) results of mice injected with luciferase-labeled HCT116 cells into the spleen after educated with PBS, SW480, LoVo, Caco2, or HCT116 exosomes, respectively. Results of quantified values of bioluminescence imaging signals are expressed as mean ± standard deviation ($n = 3$). **g.** Representative image of HE staining for liver metastases in nude mice (yellow arrows: metastatic tumour node; black arrow: normal liver cell). Scale bar = 500 μm. **h.** Number of metastatic colonies in the livers of nude mice from different groups based on living image and HE staining. (***$p < 0.001$)

we employed PKH67 (green) to label exosomes derived from CRC cells and phalloidin-TRITC (red) to label LX-2 cells. Following incubation, immunofluorescence imaging (IF) revealed the presence of PKH67-labeled spots (green) within recipient HSCs, indicating the labelled exosomes released by CRC cells were delivered to HSCs (Fig. 1d). Significantly, HSCs showed increased uptake of extracellular exosomes from high-metastatic CRC cells, underscoring the high potency of exosomes derived from high-metastatic CRC in mediating interactions between HSCs and CRC cells. Subsequently, qRT-PCR results revealed that high metastatic potential cells exosomes increased the expression of α-SMA in LX-2 cells compared with PBS and low metastatic potential cells (Fig. 1e). The IF analyses revealed that the α-SMA levels were increased after the stimulation with high-metastatic potential cells exosomes compared to low-metastatic potential cells (Fig. 1f). Migration assays demonstrated more enhanced migration of LX-2 cells in the LoVo or HCT116 group, as compared to the control group (Fig. 1g). Wound-healing assays provided further confirmation that exosomes derived from high-metastatic CRC cells significantly enhanced the migration ability of LX-2 cells (Fig. 1h).

High-metastatic CRC cell-derived exosomes exhibit potent HSCs activation in CRLM in vivo

To further determine if exosomes derived from CRC cells could stimulate the activation of LX-2 cells in vivo, an exosome-educated mice model was established (Fig. 2a). Additionally, we also established an exosome-educated CRLM model to investigate the potential of CRC cell-derived exosomes in facilitating CRLM (Fig. 2b). Initially, mice were intravenously injected by PBS, SW480 exosomes, LoVo exosomes, Caco2 exosomes, and HCT116 exosomes in the tail vein every two days for two weeks, and by a final injection of DIR-labeled exosomes to investigate the organs susceptible to CRC-derived exosomes, and then in vivo imaging was performed (Fig. 2c). Upon analyzing the fluorescence intensity across various organs, we discerned a pronounced enrichment of CRC-derived exosomes in the liver compared to other organs across all instances. Notably, exosomes originating from highly metastatic cells exhibited a greater propensity for liver internalization than those from low metastatic cells (Fig. 2d). Furthermore, IF of livers from exosome-educated mice demonstrated that exosomes derived from CRC cells, especially those with a high hepatic metastatic potential, significantly increased α-SMA expression compared to PBS (Fig. 2e). Subsequently, we administered intravenous injections of PBS, exosomes derived from SW480/LOVO and Caco2/HCT116 cells through the tail vein and then luciferase-labeled HCT116 cells were introduced into the spleen. After three weeks, in vivo imaging revealed a noteworthy elevation in fluorescence intensity within the mouse liver in the CRC-derived exosome group when compared to the PBS group. Particularly, mice educated with high-metastatic CRC-derived exosomes exhibited the highest fluorescence signal (Fig. 2f). After euthanizing the mice, liver specimens were collected to H&E staining (Fig. 2g, FIGURE S4). The findings demonstrated a significant augmentation in the number of liver metastases, particularly in those treated with high-metastatic CRC-derived exosomes, as compared to the PBS group (Fig. 2h). Hence, these findings illustrate the crucial regulatory role of CRC-derived exosomes in CRLM.

Exosomal miR-188-3p derived from high metastatic CRC cells promote HSCs activation

The elements present in exosomes, particularly miRNAs, play a pivotal role in mediating intercellular communication [34]. Therefore, the GEO database (GSE39833) was used to analyze the differentially expressed miRNAs in plasma exosomes of stage IV and I CRC patients, aiming to identify the targets associated with CRLM. We identified a total of 53 differentially expressed miRNAs in stage IV CRC patients' plasma exosomes, with 17 miRNAs down-regulated and 36 up-regulated (Fold change > 1; FDR p-value < 0.05). Based on previous research [35], miR-188-3p was selected for detailed analysis (Fig. 3a). Subsequently, we conducted validation of the miR-188-3p expression in CRC cells and exosomes (exo-miR-188-3p) within CRC cells and the findings indicated a pronounced upregulation of expression specifically in cells exhibiting high metastatic potential and their exosomes (Fig. 3b, FIGURE S5). Remarkably, miR-188-3p levels in CRC cell-conditioned medium remained unaltered after RNase A

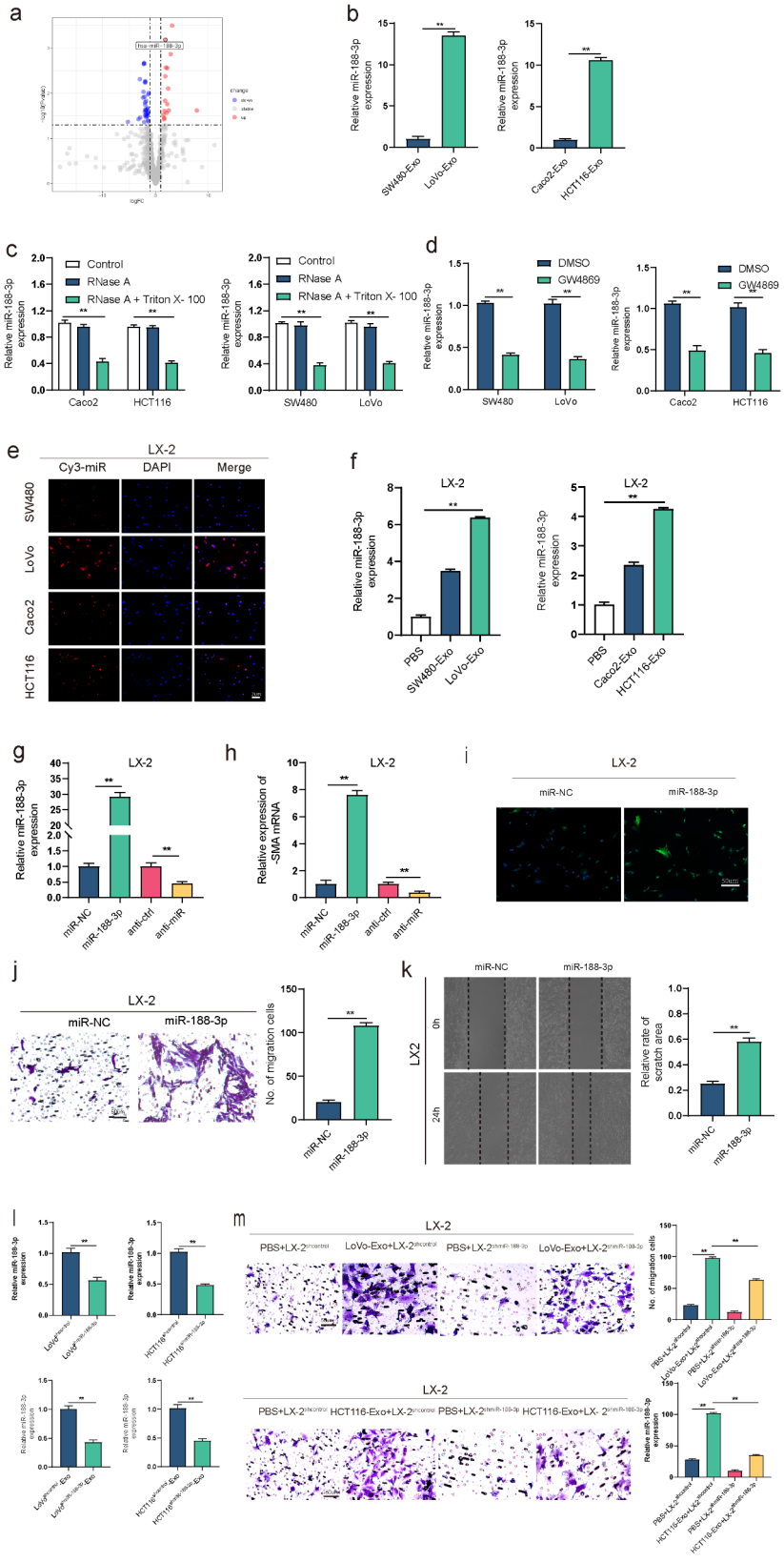

Fig. 3 (See legend on next page.)

(See figure on previous page.)

Fig. 3 MiR-188-3p-enriched exosomes derived from highly metastatic CRC cells promote HSCs activation. (**a**) Microarray analysis of miRNA expression profiles was conducted on plasma exosomes from stage IV and stage I CRC patients using the GEO database (GSE39833). (**b**) The expression levels of miR-188-3p were detected by qRT-PCR in exosomes derived from different CRC cell lines. (**c**) The expression levels of miR-188-3p were assessed using qRT-PCR in the conditioned medium (CM) of four CRC cell lines, which had been treated with CM and RNase A (2 mg/ml), alone or combined with Triton X-100 (0.1%) for 30 min. (**d**) The expression levels of miR-188-3p were assessed using qRT-PCR in the CM of four CRC cell lines, which had been treated with DMSO or an inhibitor of exosomes secretion (GW4869). (**e**) LX-2 cells were co-cultured with exosomes derived from SW480/LoVo/Caco2/HCT116 pre-transfected with Cy3-tagged miR-188-3p (red), and the red fluorescence signals in LX-2 cells were detected by fluorescence microscope. Scale bar = 2 μm. (**f**) The expression levels of miR-188-3p were assessed in LX-2 cells incubated with PBS or exosomes derived from four CRC cell lines. (**g**) The transfection efficiency of miR-188-3p mimics and inhibitor was validated in LX-2 cells. (**h**) The expression levels of α-SMA were detected by qRT-PCR in LX-2 cells after transfection of miR-188-3p mimics/NC. (**i**) Immunofluorescence images showed the levels of α-SMA in LX-2 cells after transfection of miR-188-3p mimics/NC. Scale bar = 50 μm. **j**, **k.** Transwell and wound-healing assays were employed to evaluate the effects of exogenous miR-188-3p on the migratory ability of LX-2. scale bar = 50 μm. **l.** The transfection efficiency was validated and the expression levels of miR-188-3p in exosomes were detected by qRT-PCR in LoVo and HCT116 cells after transfection with miR-188-3p inhibitor /NC. **m.** Transwell assays were employed to investigate the impact of exosomes derived from highly metastatic CRC cells (LoVo and HCT116) and miR-188-3p inhibitor on the regulation of the in vitro migratory ability of LX-2 cells. scale bar = 50 μm. (**$p < 0.01$; ***$p < 0.001$)

treatment. However, a significant decrease was observed upon treatment with RNase A combined with Triton X-100 (Fig. 3c), suggesting that extracellular miR-188-3p was primarily encapsulated within a membrane instead of being directly released. Notably, the expression levels of miR-188-3p exhibited a decrease in the CM from CRC cells upon treatment with exosome-depleted CM using GW4869, an inhibitor of exosome secretion (Fig. 3d). Additionally, co-cultured Cy3 (red)-tagged miR-188-3p exosomes originating from CRC cells and LX-2 cells the presence of fluorescently labelled miR-188-3p in LX-2 cells was observed, suggesting the transfer of miR-188-3p from CRC cells to HSCs through exosomes. Importantly, a more substantial quantity of miR-188-3p exosomes from highly metastatic CRC cells was taken up (Fig. 3e). Moreover, we explored the expression of miR-188-3p in LX-2 cells during co-culture with exosomes from CRC cells. A significant increase in miR-188-3p levels within LX-2 cells was detected when exposed to exosomes derived from high metastatic CRC cells, in contrast to those from low metastatic CRC cells (Fig. 3f). To determine HSC activation associated with miR-188-3p, miR-188-3p mimics and inhibitor was introduced into LX-2 cells (Fig. 3g). Overexpression of miR-188-3p resulted in an increased expression of α-SMA, indicative of heightened HSC activation. In contrast, the inhibition of miR-188-3p led to a decrease in α-SMA expression (Fig. 3h). The IF analysis demonstrated a notable enhancement in the fluorescence intensity of α-SMA in LX-2 cell in the miR-188-3p overexpression group (Fig. 3i). Furthermore, the overexpression of miR-188-3p facilitated the migration of LX-2 cells (Fig. 3j, k). The transfection efficiency of miR-188-3p inhibitor was confirmed in highly metastatic cells and their corresponding exosomes (Fig. 3l). Transwell assays revealed that anti-miR-188-3p could mitigate the impact of exosomes derived from highly metastatic CRC cells on the activation of LX-2 cells (Fig. 3m, n).

Exosomal miR-188-3p from CRC cells activates HSCs by targeting PHLPP2 and activating the AKT/mTOR signalling pathway

According to TargetScan Human version 7.2 data, an alignment was observed between the sequence of miR-188-3p and the 3′-UTR of pleckstrin homology domain and leucine-rich repeat protein phosphatase 2 (PHLPP2), indicating the potential targeting of PHLPP2 by exosomal miR-188-3p derived from CRC cells during the activation of HSCs (Fig. 4a). After co-transfecting miR-188-3p mimics, inhibitor, and their corresponding controls, luciferase vectors containing wild-type or mutant versions of the binding sites were employed for additional confirmation. As illustrated in Fig. 4b, relative to the control groups, luciferase activity in LX-2 cells transfected with miR-188-3p mimics or inhibitor exhibited a significant decrease or increase, respectively, in the group co-transfected with the PHLPP2 wild-type binding site vector compared to the PHLPP2 mutant-type binding site vector. Further experiments in LX-2 cells demonstrated a significant inhibition or promotion of PHLPP2 expression at both mRNA and protein levels upon overexpression or knockdown of miR-188-3p, as compared to their negative controls (Fig. 4c). Consistently, similar expression patterns were observed in LX-2 cells following pretreatment with exosomes derived from SW480/LoVo cells pre-transfected with miR-188-3p mimics or inhibitor (Fig. 4d). The overexpression efficiency of PHLPP2 overexpression plasmid was validated in LX-2 cells (Fig. 4e). Transwell assays revealed that the elevated expression of PHLPP2 led to a reduction in the number of migrating LX-2 cells, partially attenuating the stimulatory effect of miR-188-3p on LX-2 cell migration (Fig. 4f). Collectively, these findings imply that the introduction of exogenous miR-188-3p results in the downregulation of PHLPP2 expression by specifically targeting its 3'-UTR in LX-2 cells.

Moreover, pre-transfection of SW480/LoVo cells was conducted with either miR-188-3p mimic or anti-miR-188-3p, and subsequently, LX-2 cells were co-cultured

with exosomes derived from the previously mentioned cells. WB analyses revealed a notable increase in p-AKT and p-mTOR expression, accompanied by a reduction in PHLPP2 levels within LX-2 cells upon exposure to exosomes carrying miR-188-3p derived from CRC cells (Fig. 4g, h). These findings suggest that miR-188-3p-enriched exosomes directly activate HSCs by targeting PHLPP2 through the activation of the AKT/mTOR signalling pathway.

HSCs activated by CRC-derived exosomal miR-188-3p facilitate CRLM

Our previous study has shown that aHSCs lead to a significant upregulation in collagen synthesis and ECM, and have been shown to promote CRC cell proliferation and migration. Hence, we examined whether exosomal miR-188-3p-activated HSCs could actively facilitate CRLM. Tanswell experiments demonstrate that miR-188-3p-activated LX-2 significantly enhances the migratory ability of CRC cells (Fig. 5a). Subsequently, LX-2 cells underwent co-cultivation with exosomes from SW480 cells with miR-188-3p mimics facilitated HCT116 cell migration in comparison to control. While relative to control, LX-2 cells underwent co-cultivation with exosomes from LoVo cells with miR-188-3p inhibitor exhibited a great reduction in the number of HCT116 cells (Fig. 5b). Notably, exosomes originating from LoVo cells exhibited a greater propensity for liver internalization compared to those from SW480 cells (Fig. 5c). Moreover, exosomes originating from SW480 cells with miR-188-3p mimics exhibited a notable enhancement in the fluorescence intensity of α-SMA in LX-2 cell, while those derived from LoVo cells with miR-188-3p inhibitor demonstrated a marked decrease in liver fluorescence signals (Fig. 5d). Concurrently, a CRLM model educated by exosomes was employed to explore the function of exosomal miR-188-3p in CRLM. The IVIS results demonstrated a marked increase in liver fluorescence signals upon exposure to exosomes from CRC cells with miR-188-3p mimics, as compared to controls. Conversely, exosomes from CRC cells with miR-188-3p inhibitor exhibited a reduction in the fluorescence signal (Fig. 5e). Consistently, H&E staining indicated that exposure to exosomes from CRC cells with miR-188-3p mimics facilitated liver metastasis in comparison to control. Conversely, the education with exosomes from CRC cells with miR-188-3p inhibitor resulted in the inhibition of liver metastasis (Fig. 5f, g & FIGURE S6). These results suggest that exosomal miR-188-3p triggers the activation of HSCs, thereby facilitating the promotion of liver metastasis.

Exosomal miR-188-3p in plasma of CRC patients correlates with liver metastasis

Firstly, qRT-PCR analysis was performed on 214 freshly gathered CRC tissue samples, which demonstrated a noteworthy elevation in the expression of miR-188-3p in tissues derived from stage III-IV tumors compared to stage I-II tumors (Fig. 6a). Then, we investigated miR-188-3p expression in plasma exosomes (Fig. 6b, c) and observed that plasma exosomes from CRC patients with liver metastasis (LM) exhibited higher expression levels of miR-188-3p than those without LM (Fig. 6d). Additionally, there was a positive correlation between miR-188-3p expression in plasma exosomes and tumor size, advanced AJCC stage (TABLE S3). Cox proportional hazard regression analysis showed that the increased expression of plasma exosomal miR-188-3p in CRC patients was an independent predictor of DFS and OS (TABLES S4 and S5). According to Kaplan-Meier survival analysis, patients with higher miR-188-3p expression in plasma exosomes displayed significantly reduced DFS and OS rates (Fig. 6e, f).

Discussion

Recently, the incidence and mortality rates of cancer have significantly increased, with CRC being one of the most prevalent cancers worldwide [36]. As highlighted in the study, the global burden of cancer, driven by various risk factors, is a major contributor to the increasing incidence and mortality rates of CRC, reinforcing the urgent need for more effective prevention and treatment strategies [37]. Meanwhile, research on the pathogenesis and treatment of primary HCC has progressed significantly [38–41]. In contrast, studies on secondary liver cancer due to CRLM are relatively recent, and the mechanisms remain unclear. Therefore, understanding the molecular mechanisms behind CRLM, especially the interaction between miR-188-3p and HSCs, has important clinical implications.

CRLM is widely acknowledged as a complex biological cascade characterized by multifactorial involvement, genetic alterations, and a multi-step developmental progression [42, 43], and the liver's microenvironment plays a crucial role in influencing the formation of the final metastatic lesions, ultimately determining the ability of CRC cells to successfully colonize it. Numerous studies indicate that primary tumors can induce the formation of a favourable environment for metastasis at distant organs, known as the PMN, facilitating the process of metastasis [14, 44]. The PMN is a supportive and receptive tissue microenvironment whose characteristics determine whether circulating tumor cells can implant, survive, and form metastatic lesions upon reaching the metastatic site, or enter a dormant state. The formation of the PMN is crucial for distant organ metastasis, including liver

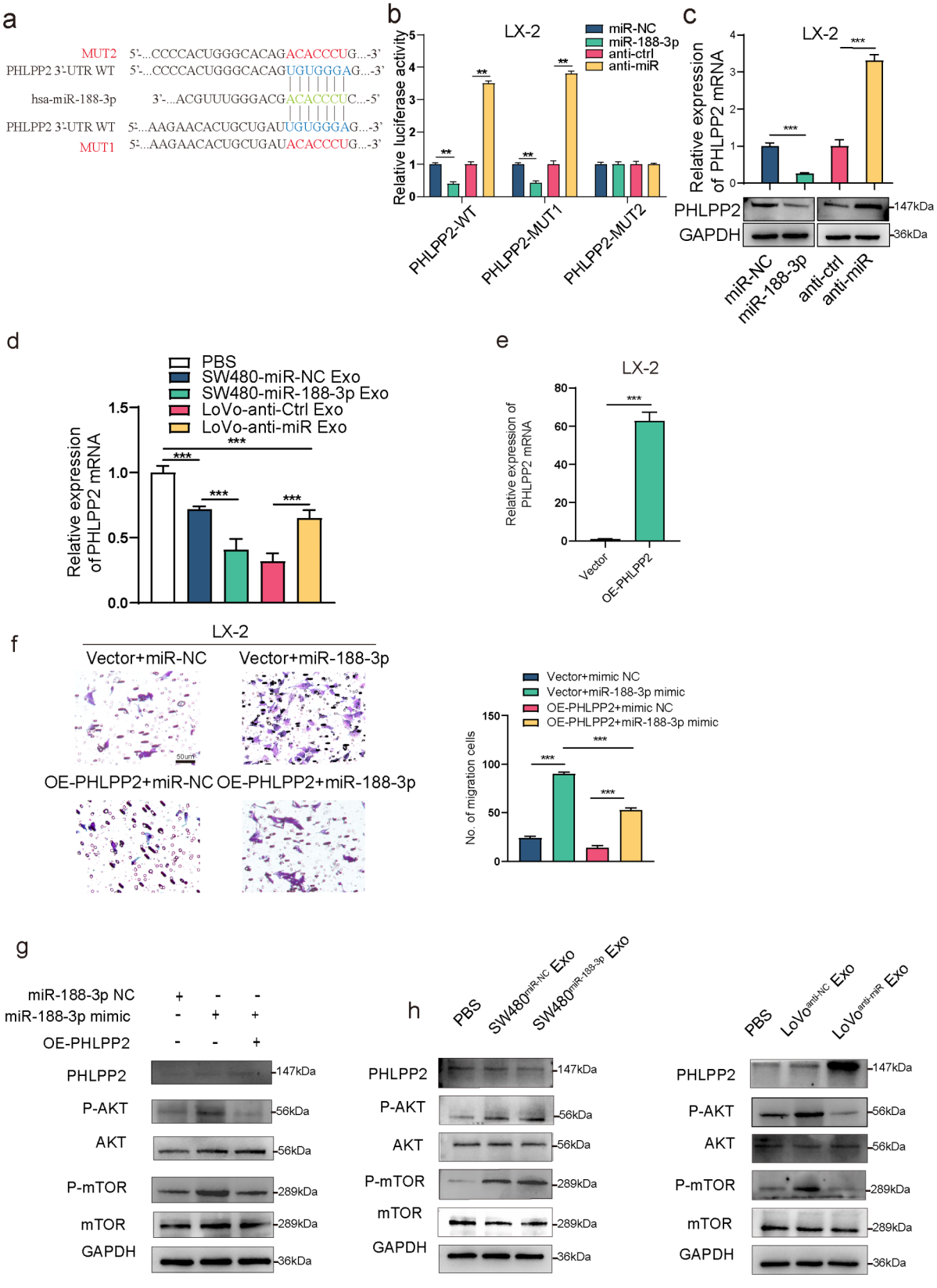

Fig. 4 (See legend on next page.)

(See figure on previous page.)

Fig. 4 CRC cell-derived exosome miR-188-3p activates HSCs directly by targeting PHLPP2 and activating the AKT/mTOR signalling pathway in HSCs. (**a**) Predicted binding sites between miR-188-3p and the 3′-UTR of the wild-type and mutant PHLPP2 gene. (**b**) Relative luciferase activity of 3′UTR-PHLPP2-luc constructs in LX-2 cells after transfection of miR-188-3p mimics/NC and inhibitor/NC. (**c**) qRT-PCR and WB analysis were employed to assess the impact of exogenous miR-188-3p on the expression of PHLPP2 in LX-2 cells. (**d**) qRT-PCR analysis was used to examine the effect of exosomes derived from SW480 and LoVo CRC cells rich in miR-188-3p on PHLPP2 expression in LX-2 cells. (**e**) The transfection efficiency was validated and the expression levels of PHLPP2 were detected by qRT-PCR in LX-2 cells after transfection with PHLPP2 mimics/NC. (**f**) Transwell assays were applied to verify the combined effect of miR-188-3p and PHLPP2 overexpression on the invasion of LX-2. Scale bar = 50 μm. (**g**) LX-2 cells were pre-transfected with miR-188-3p mimic, and then co-cultured with PHLPP2 mimics. The combined effects of exogenous miR-188-3p/ PHLPP2 mimics on the expression of AKT/m-TOR pathway components were determined by WB analysis, respectively. (**h**) WB analysis was used to examine the effect of exosomes derived from CRC cells rich in miR-188-3p on the AKT/mTOR pathway components in LX-2. (**$p < 0.01$; ***$p < 0.001$)

metastasis in CRC, and has attracted increasing attention. In this study, we validated exosomal miR-188-3p derived from high metastatic CRC cells through activated HSCs to form the PMN, and we also established that activated HSCs, in turn, play a pivotal role in promoting liver metastasis. These findings significantly contribute to our understanding of the complex interaction between cancer cells and the liver microenvironment, emphasizing the role of HSCs in promoting CRLM. HSCs, as the main stromal cells in the liver, significantly impacted the progression and intensification of metastasis. HSCs play a vital role in establishing a PMN and are instrumental in the recruitment of CRC cells [45]. aHSCs can release chemokines when exposed to cancer cell stimulation and liver damage, which can facilitate the invasion and proliferation of CRC [46]. Previous studies have shown a notable increase in the activation of HSCs in CRLM tissues [47, 48], which suggests that the activation of HSC leading to alterations in the microenvironment may be one of the primary factors contributing to liver metastases in CRC and is also identified as a significant factor causing a high incidence of CRLM. These findings underscore the importance of HSCs activation in metastasis, highlighting the need for targeted therapies that can modulate the liver microenvironment. Our study demonstrates that exosomes from CRC cells with high metastatic potential efficiently activate HSCs, leading to the formation of the PMN, which significantly enhances the occurrence of CRLM.

Exosomes are emerging as important players in intercellular communication between cancer cells and stromal cells in the PMN [14, 49, 50]. Exosome-mediated transfer of miRNAs into specific recipient cells via their cargos to form PMN contributed to tumor metastasis [27, 51, 52]. It has been shown that tumor-derived exosomal miR-1247-3p induces cancer-associated fibroblast activation to foster metastasis of liver cancer [53]. Exosome-mediated transfer of cancer-secreted miR-105 efficiently destroys tight junctions by targeting ZO-1 to promote breast cancer metastasis [54]. miR-188-3p has been reported as a cancer-promoting miRNA that correlated with poor prognosis of CRC patients [35]. However, the molecular mechanism through which miR-188-3p regulates CRC metastasis has not been delineated. This is the first study to explore the molecular mechanisms by which miR-188-3p regulates CRC liver metastasis through exosome-mediated HSC activation, a novel finding that adds to the growing body of knowledge about the role of non-coding RNAs in cancer progression. In the present study, exosomes were used, which are considered a significant factor within the PMN, to investigate the specific function of miR-188-3p in regulating the crosstalk between the primary CRC tumor site and liver metastatic loci. The results revealed that miR-188-3p in exosomes secreted by CRC cells could promote the migratory ability of HSCs, as determined by wound-healing and Transwell assays. The enhanced migratory capacity of HSCs may be a favourable factor for the metastasis of CRC cells. Furthermore, we found that exosomes from high metastatic CRC cells, enriched with miR-188-3p, could stimulate HSCs by directly suppressing PHLPP2, leading to the activation of the AKT/mTOR signalling pathway and ultimately forming the PMN. Cancer therapies that target the pre-metastatic niche hold promise as effective strategies for combating metastasis. Inhibiting the S1PR1-STAT3 signaling axis in myeloid cells disrupts pre-metastatic niche formation and impedes cancer metastasis [55]. Our results showed that blocking the release of exosomal miR-188-3p from CRC cells reduced HSC migration and subsequent CRC metastasis, suggesting that miR-188-3p could serve as a therapeutic target to intervene in CRC metastasis. These findings offer a new molecular target for CRLM, which could facilitate the development of more effective diagnostic and therapeutic approaches.

Recent research highlights the growing importance of exosomal biomarkers in diagnosing cancer and evaluating prognosis. Previous studies showed serum exosomal miR-106b-3p can serve as effective indicators of CRLM and exosomal miR-181a-5p in the serum were related to a poor prognosis in CRLM patients [47, 56]. Here, our findings indicate that the level of miR-188-3p in plasma exosomes is associated with CRLM. The survival analysis indicated that CRC patients with overexpressed miR-188-3p had a shorter DFS and OS. Furthermore, CRLM patients with high exosomal miR-188-3p levels exhibited poorer DFS and OS. Our clinical data collectively indicate that measuring plasma exosomal miR-188-3p levels

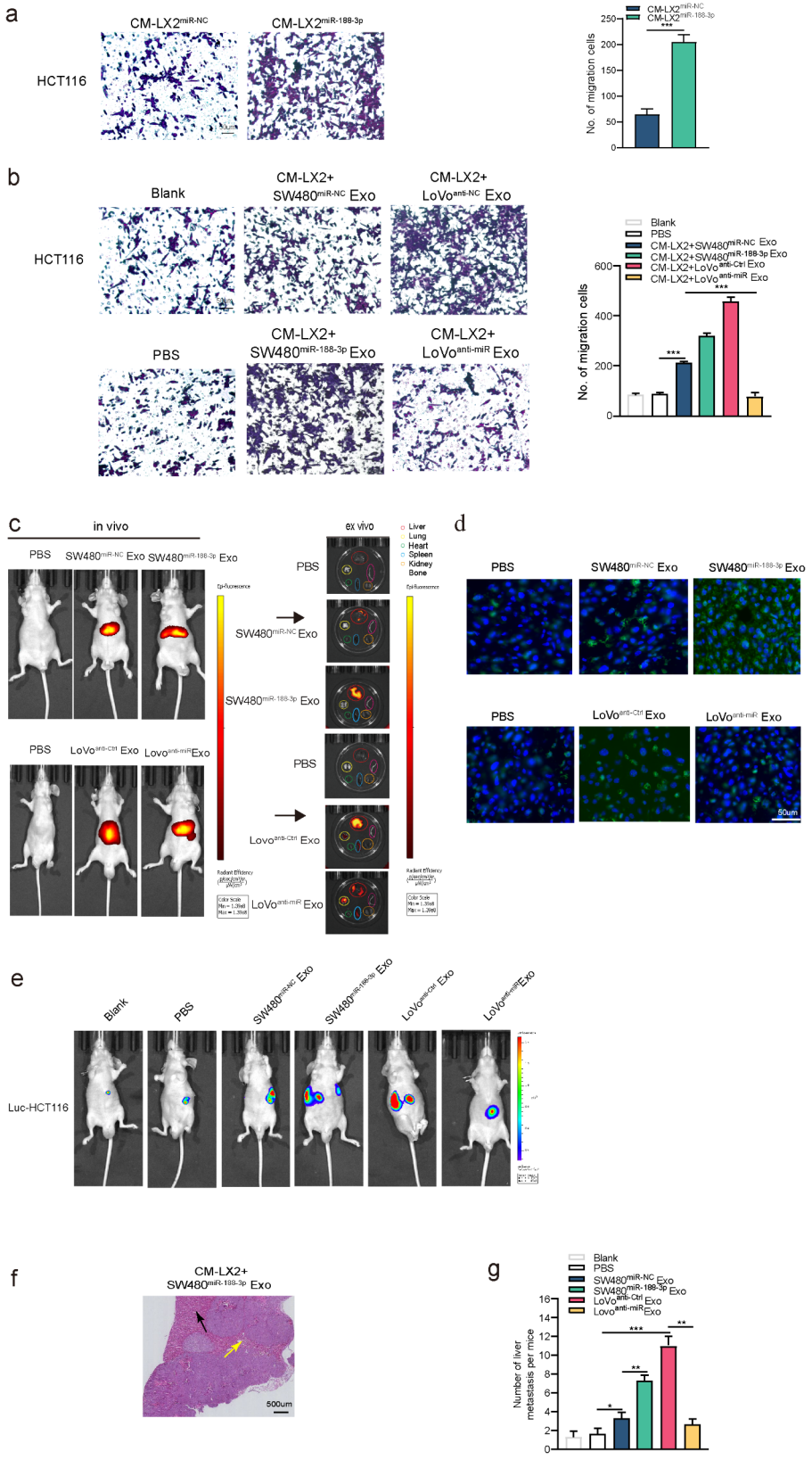

Fig. 5 (See legend on next page.)

(See figure on previous page.)

Fig. 5 HSCs Activated by CRC-derived exosome miR-188-3p facilitate CRC progression. (**a**) LX-2 cells were first transfected with miR-188-3p mimic or the respective control. Then, CM from these transfected LX-2 cells were added to HCT116 cell cultures, and transwell assays were used to examine the effect of exogenous miR-188-3p on the migration of CRC cells. (**b**) SW480/LoVo cells were pre-transfected with miR-188-3p or anti-miR-188-3p, respectively and exosomes were isolated and LX-2 cells were co-cultured with these exosomes. Then the CM of these LX-2 cells was added to HCT116 cells, respectively. The effect of α-HSCs on the migration of CRC cells was determined using transwell assays in vitro. (**c**) Representative in vivo imaging system (IVIS) results of mice educated with PBS or SW480, LoVo cells pre-transfected with miR-188-3p or anti-miR-188-3p, respectively. (**d**) Immunofluorescence was used to detect the activation of LX-2 trained under different conditions in the liver of nude mice. **e**, **f.** Representative images of live imaging (**e**) and HE staining (**f**) of the liver metastases in nude mice. **g.** Quantification of metastatic colonies in the livers of nude mice across various groups based on live imaging and HE staining. (*$p < 0.05$; **$p < 0.01$; ***$p < 0.001$)

could be beneficial for predicting CRLM and selecting high-risk patients subject to CRLM for early intervention.

While the present study yields intriguing findings, it is not without limitations. In this study, we explored the positive feedback effect of α-SMA on CRC cells to promote liver metastasis. However, the specific mechanisms underlying this process remain to be further investigated. Furthermore, the mechanism by which miR-188-3p is encapsulated into exosomes has not been extensively studied.

In future studies, we will delve into the molecular mechanisms of CRC cell-derived exosomes in regulating HSCs, as well as the molecular mechanisms and clinical significance of CRC cell interactions with PMNs, aiming to provide new perspectives for understanding the metastatic process of CRC.

Conclusion

In summary, our study demonstrated that miR-188-3p-containing exosomes derived from highly metastatic CRC cells activate HSCs through AKT/mTOR signaling, leading to the establishment of a PMN in the liver. In turn, activated HSCs promoted CRC liver metastasis by remodeling the tumor microenvironment. This study reveals a novel mechanism of CRLM, offering new insights into the molecular interplay between CRC cells and HSCs. Furthermore, these findings may contribute to developing new diagnostic markers and therapeutic strategies for predicting and preventing CRLM,

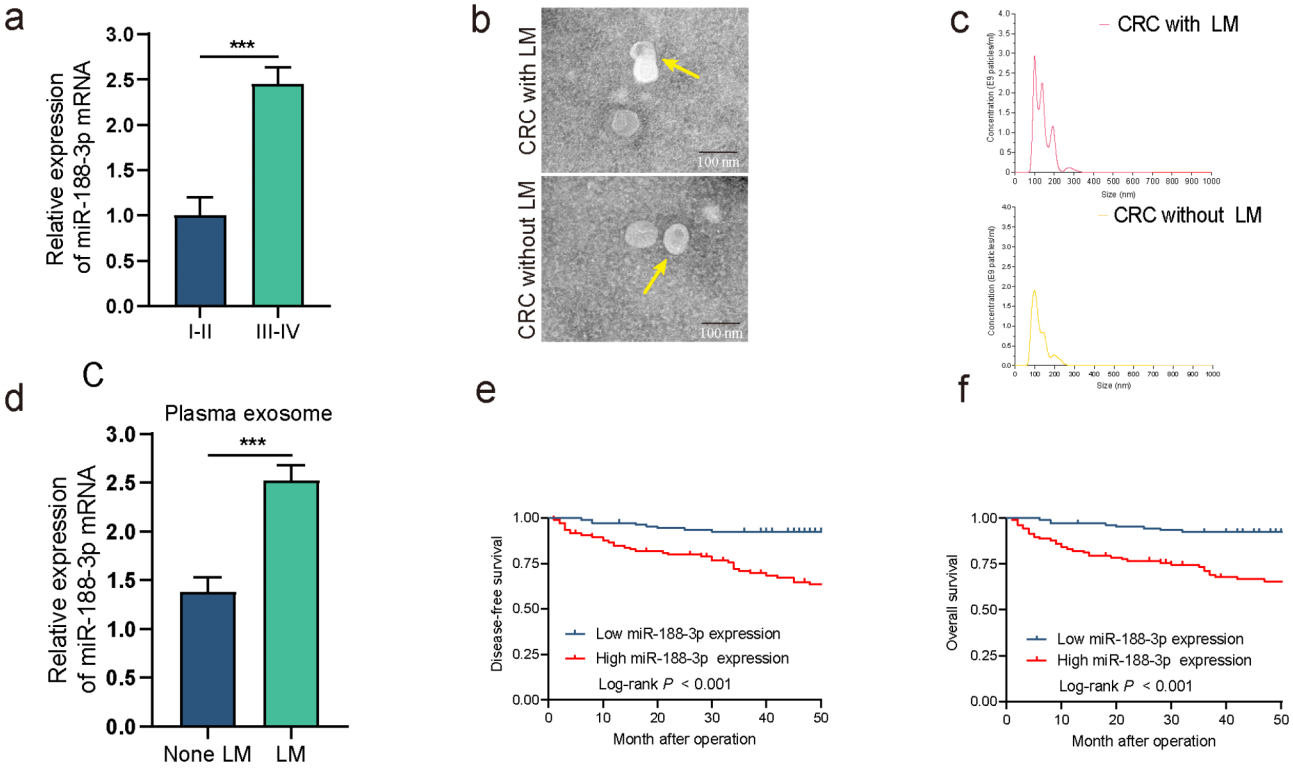

Fig. 6 Exosomal miR-188-3p in plasma of CRC patients correlates with liver metastasis. **a**. The expression levels of miR-188-3p were assessed in CRC patients with stage I-II and stage III-IV tumors using qRT-PCR. **b**, **c.** Plasma exosomes were additionally identified through electron microscopy (**b**) and Nanosight particle tracking analysis (**c**). **d.** qRT-PCR assays were employed to assess the expression of miR-188-3p in plasma exosomes obtained from CRC patients without liver metastasis (None LM) and those with liver metastasis (LM). **e**, **f.** Kaplan-Meier survival analysis and log-rank tests were employed to assess the correlations between miR-188-3p in plasma exosomes and DFS (**e**) and OS (**f**) in CRC patients. (***$p < 0.001$)

which remains a significant clinical challenge in CRC management.

Abbreviations

aHSC	Activated hepatic stellate cell
α-SMA	α-smooth muscle actin
CD9	Cluster of Differentiation 9
CRC	Colorectal cancer
CRLM	Colorectal live metastasis
DAPI	4′,6-diamidino-2-phenylindole
DFS	Disease-free survival
GAPDH	Glyceraldehyde 3-phosphate dehydrogenase
HSC	Hepatic stellate cell
TSG101	Tumor susceptibility gene 101 protein
PMN	Pre-metastatic niche
OS	Overall survival
qRT-PCR	Quantitative real-time polymerase Chain reaction
WB	Western blotting

Supplementary Information

The online version contains supplementary material available at https://doi.org/10.1186/s12967-025-06334-4.

Supplementary Material 1

Acknowledgements
None.

Author contributions
Tao Li, Taiyuan Li and Yahang Liang conducted the experiments, analyzed the data, and prepared the manuscript. Yuli Yuan contributed to the bioinformatics analysis. Yang Liu and Yao Yao were involved in interpreting the information, editing, and critically revising the manuscript. Xiong Lei conceived the study and provided overall direction for the project. All authors contributed to the article and approved the final submitted version.

Funding
This work was supported by Natural Science Foundation of China (grant no. 81860519; 82160561), key project of Natural Science Foundation of Jiangxi, China (grant no. 20192ACBL21043).

Data availability
The data that support the findings of this study are available from the corresponding author upon reasonable request.

Declarations

Ethics approval and consent to participate
Informed consent and approval were obtained from all the patients and the Ethics Committee of the First Affiliated Hospital of Nanchang University. All the animal studies were performed following the Guidelines for the Care and Use of Laboratory Animals and were approved by the Ethics Committee of the First Affiliated Hospital of Nanchang University.

Consent for publication
Not applicable.

Competing interests
The authors declare that they have no competing interests.

Author details
[1]Department of General surgery, The First Affiliated Hospital, Jiangxi Medical College, Nanchang University, Nanchang 330006, Jiangxi, China
[2]Gastrointestinal Surgical Institute, Nanchang University, Nanchang 330006, Jiangxi, China

Received: 18 December 2024 / Accepted: 1 March 2025
Published online: 25 March 2025

References

1. Siegel RL, Giaquinto AN, Jemal A. Cancer statistics, 2024. CA Cancer J Clin. 2024;74(1):12–49.
2. Siegel RL, Wagle NS, Cercek A, Smith RA, Jemal A. Colorectal cancer statistics, 2023. CA Cancer J Clin. 2023;73(3):233–54.
3. Eng C, Yoshino T, Ruíz-García E, Mostafa N, Cann CG, O'Brian B, et al. Colorectal cancer. Lancet. 2024;404(10449):294–310.
4. Cohen R, Raeisi M, Chibaudel B, Shi Q, Yoshino T, Zalcberg JR, et al. Prognostic value of liver metastases in colorectal cancer treated by systemic therapy: an arcad pooled analysis. Eur J Cancer. 2024;207:114160.
5. Sun H, Sun L, Ke X, Liu L, Li C, Jin B, et al. Prediction of clinical precision chemotherapy by patient-derived 3d bioprinting models of colorectal cancer and its liver metastases. Adv Sci (Weinh). 2024;11(2):e2304460.
6. Zhou H, Liu Z, Wang Y, Wen X, Amador EH, Yuan L, et al. Colorectal liver metastasis: molecular mechanism and interventional therapy. Signal Transduct Target Ther. 2022;7(1):70.
7. Song M. Global epidemiology and prevention of colorectal cancer. Lancet Gastroenterol Hepatol. 2022;7(7):588–90.
8. Xu W, Liu J, Liu Q, Xu J, Zhou L, Liang Z, et al. Nfe2-driven neutrophil polarization promotes pancreatic cancer liver metastasis progression. Cell Rep. 2025;44(2):115226.
9. Shi LL, Chen Y, Xie MX, Chen QZ, Qiao XW, Cheng QH et al. Ube2t/cdc42/cd276 signaling axis mediates brain metastasis of triple-negative breast cancer via lysosomal autophagy. J Immunother Cancer. 2025;13(2).
10. Tey SK, Wong SWK, Chan JYT, Mao X, Ng TH, Yeung CLS, et al. Patient pigr-enriched extracellular vesicles drive cancer stemness, tumorigenesis and metastasis in hepatocellular carcinoma. J Hepatol. 2022;76(4):883–95.
11. Valastyan S, Weinberg RA. Tumor metastasis: molecular insights and evolving paradigms. Cell. 2011;147(2):275–92.
12. Malki A, ElRuz RA, Gupta I, Allouch A, Vranic S, Al Moustafa AE. Molecular mechanisms of colon cancer progression and metastasis: recent insights and advancements. Int J Mol Sci. 2020;22(1).
13. Wang Y, Zhong X, He X, Hu Z, Huang H, Chen J, et al. Liver metastasis from colorectal cancer: pathogenetic development, immune landscape of the tumour microenvironment and therapeutic approaches. J Exp Clin Cancer Res. 2023;42(1):177.
14. Liu Y, Cao X. Characteristics and significance of the pre-metastatic niche. Cancer Cell. 2016;30(5):668–81.
15. Cui Y, Chang Y, Ma X, Sun M, Huang Y, Yang F, et al. Ephrin a1 stimulates ccl2 secretion to facilitate premetastatic niche formation and promote gastric cancer liver metastasis. Cancer Res. 2025;85(2):263–76.
16. Jiang X, Wang J, Lin L, Du L, Ding Y, Zheng F, et al. Macrophages promote pre-metastatic niche formation of breast cancer through aryl hydrocarbon receptor activity. Signal Transduct Target Ther. 2024;9(1):352.
17. Zhao Y, Yu H, Li J, Qian J, Li M, Zhang X, et al. A glucose-enriched lung pre-metastatic niche triggered by matrix stiffness-tuned exosomal mirnas in hepatocellular carcinoma. Nat Commun. 2025;16(1):1736.
18. Zhang C, Wang XY, Zhang P, He TC, Han JH, Zhang R, et al. Cancer-derived exosomal hspc111 promotes colorectal cancer liver metastasis by reprogramming lipid metabolism in cancer-associated fibroblasts. Cell Death Dis. 2022;13(1):57.
19. Zhang Y, Li X, Chen H, Li J, Guo X, Fang Y, et al. Cancer cell-derived exosomal mir-500a-3p modulates hepatic stellate cell activation and the immunosuppressive microenvironment. Adv Sci (Weinh). 2025;12(2):e2404089.
20. Du Y, Wu S, Xi S, Xu W, Sun L, Yan J, et al. Ash1l in hepatoma cells and hepatic stellate cells promotes fibrosis-associated hepatocellular carcinoma by modulating tumor-associated macrophages. Adv Sci (Weinh). 2024;11(45):e2404756.
21. Kang N, Gores GJ, Shah VH. Hepatic stellate cells: partners in crime for liver metastases? Hepatology. 2011;54(2):707–13.
22. Zhang DY, Goossens N, Guo J, Tsai MC, Chou HI, Altunkaynak C, et al. A hepatic stellate cell gene expression signature associated with outcomes in hepatitis C cirrhosis and hepatocellular carcinoma after curative resection. Gut. 2016;65(10):1754–64.
23. Affo S, Yu LX, Schwabe RF. The role of cancer-associated fibroblasts and fibrosis in liver cancer. Annu Rev Pathol. 2017;12:153–86.
24. Ahmad SA, Berman RS, Ellis LM. Biology of colorectal liver metastases. Surg Oncol Clin N Am. 2003;12(1):135–50.
25. Deng L, Li T, Liao Y, Liu S, Xie Z, Huang Z, et al. Peritumoral activated hepatic stellate cells are associated with hepatic recurrence for resectable colorectal adenocarcinoma liver metastasis following resection. Oncol Lett. 2020;20(6):287.

26. Kalluri R, LeBleu VS. The biology, function, and biomedical applications of exosomes. Science. 2020;367(6478).
27. Li B, Cao Y, Sun M, Feng H. Expression, regulation, and function of exosome-derived mirnas in cancer progression and therapy. Faseb J. 2021;35(10):e21916.
28. Zhang L, Zhang S, Yao J, Lowery FJ, Zhang Q, Huang WC, et al. Microenvironment-induced pten loss by exosomal microrna primes brain metastasis outgrowth. Nature. 2015;527(7576):100–4.
29. Watany M, Badawi R, Elkhalawany W, Abd-Elsalam S. Study of dickkopf-1 (dkk-1) gene expression in hepatocellular carcinoma patients. J Clin Diagn Res. 2017;11(2):Oc32–4.
30. Elhendawy M, Abdul-Baki EA, Abd-Elsalam S, Hagras MM, Zidan AA, Abdel-Naby AY, et al. Microrna signature in hepatocellular carcinoma patients: identification of potential markers. Mol Biol Rep. 2020;47(7):4945–53.
31. Lei X, Deng L, Liu D, Liao S, Dai H, Li J, et al. Arhgef7 promotes metastasis of colorectal adenocarcinoma by regulating the motility of cancer cells. Int J Oncol. 2018;53(5):1980–96.
32. Qiu S, Xie L, Lu C, Gu C, Xia Y, Lv J, et al. Gastric cancer-derived exosomal mir-519a-3p promotes liver metastasis by inducing intrahepatic m2-like macrophage-mediated angiogenesis. J Exp Clin Cancer Res. 2022;41(1):296.
33. Kalluri R. The biology and function of fibroblasts in cancer. Nat Rev Cancer. 2016;16(9):582–98.
34. Wang M, Yu F, Ding H, Wang Y, Li P, Wang K. Emerging function and clinical values of exosomal micrornas in cancer. Mol Ther Nucleic Acids. 2019;16:791–804.
35. Pichler M, Stiegelbauer V, Vychytilova-Faltejskova P, Ivan C, Ling H, Winter E, et al. Genome-wide mirna analysis identifies mir-188-3p as a novel prognostic marker and molecular factor involved in colorectal carcinogenesis. Clin Cancer Res. 2017;23(5):1323–33.
36. Kocarnik JM, Compton K, Dean FE, Fu W, Gaw BL, Harvey JD, et al. Cancer incidence, mortality, years of life lost, years lived with disability, and disability-adjusted life years for 29 cancer groups from 2010 to 2019: a systematic analysis for the global burden of disease study 2019. JAMA Oncol. 2022;8(3):420–44.
37. The global burden of cancer attributable to risk factors. 2010-19: a systematic analysis for the global burden of disease study 2019. Lancet. 2022;400(10352):563–91.
38. Sheta E, El-Kalla F, El-Gharib M, Kobtan A, Elhendawy M, Abd-Elsalam S, et al. Comparison of single-session transarterial chemoembolization combined with microwave ablation or radiofrequency ablation in the treatment of hepatocellular carcinoma: a randomized-controlled study. Eur J Gastroenterol Hepatol. 2016;28(10):1198–203.
39. Elwan N, Salem ML, Kobtan A, El-Kalla F, Mansour L, Yousef M, et al. High numbers of myeloid derived suppressor cells in peripheral blood and ascitic fluid of cirrhotic and Hcc patients. Immunol Invest. 2018;47(2):169–80.
40. El-Gebaly F, Abou-Saif S, Elkadeem M, Helmy A, Abd-Elsalam S, Yousef M, et al. Study of serum soluble programmed death ligand 1 as a prognostic factor in hepatocellular carcinoma in Egyptian patients. Curr Cancer Drug Targets. 2019;19(11):896–905.
41. Abdel Ghafar MT, Morad MA, El-Zamarany EA, Ziada D, Soliman H, Abd-Elsalam S, et al. Autologous dendritic cells pulsed with lysate from an allogeneic hepatic cancer cell line as a treatment for patients with advanced hepatocellular carcinoma: a pilot study. Int Immunopharmacol. 2020;82:106375.
42. Zarour LR, Anand S, Billingsley KG, Bisson WH, Cercek A, Clarke MF, et al. Colorectal cancer liver metastasis: evolving paradigms and future directions. Cell Mol Gastroenterol Hepatol. 2017;3(2):163–73.
43. Chen H, Zhai C, Xu X, Wang H, Han W, Shen J. Multilevel heterogeneity of colorectal cancer liver metastasis. Cancers (Basel). 2023;16(1).
44. Chin AR, Wang SE. Cancer tills the premetastatic field: mechanistic basis and clinical implications. Clin Cancer Res. 2016;22(15):3725–33.
45. Patel BY, Bhome R, Liu DSK, Giovannetti E, Merali N, Primrose JN, et al. Cancer cell-derived extracellular vesicles activate hepatic stellate cells in colorectal cancer. Expert Rev Mol Diagn. 2023;23(10):843–9.
46. Chu X, Jin Q, Chen H, Wood GC, Petrick A, Strodel W, et al. Ccl20 is up-regulated in non-alcoholic fatty liver disease fibrosis and is produced by hepatic stellate cells in response to fatty acid loading. J Transl Med. 2018;16(1):108.
47. Zhao S, Mi Y, Zheng B, Wei P, Gu Y, Zhang Z, et al. Highly-metastatic colorectal cancer cell released mir-181a-5p-rich extracellular vesicles promote liver metastasis by activating hepatic stellate cells and remodelling the tumour microenvironment. J Extracell Vesicles. 2022;11(1):e12186.
48. Li F, Zhan L, Dong Q, Wang Q, Wang Y, Li X, et al. Tumor-derived exosome-educated hepatic stellate cells regulate lactate metabolism of hypoxic colorectal tumor cells via the il-6/stat3 pathway to confer drug resistance. Onco Targets Ther. 2020;13:7851–64.
49. Yan W, Wu X, Zhou W, Fong MY, Cao M, Liu J, et al. Cancer-cell-secreted exosomal mir-105 promotes tumour growth through the myc-dependent metabolic reprogramming of stromal cells. Nat Cell Biol. 2018;20(5):597–609.
50. Guo Y, Ji X, Liu J, Fan D, Zhou Q, Chen C, et al. Effects of exosomes on pre-metastatic niche formation in tumors. Mol Cancer. 2019;18(1):39.
51. Martinez-Espinosa I, Serrato JA, Ortiz-Quintero B. The role of exosome-derived microrna on lung cancer metastasis progression. Biomolecules. 2023;13(11).
52. Fanale D, Corsini LR, Bono M, Randazzo U, Barraco N, Brando C, et al. Clinical relevance of exosome-derived micrornas in ovarian cancer: looking for new tumor biological fingerprints. Crit Rev Oncol Hematol. 2024;193:104220.
53. Fang T, Lv H, Lv G, Li T, Wang C, Han Q, et al. Tumor-derived exosomal mir-1247-3p induces cancer-associated fibroblast activation to foster lung metastasis of liver cancer. Nat Commun. 2018;9(1):191.
54. Zhou W, Fong MY, Min Y, Somlo G, Liu L, Palomares MR, et al. Cancer-secreted mir-105 destroys vascular endothelial barriers to promote metastasis. Cancer Cell. 2014;25(4):501–15.
55. Deng J, Liu Y, Lee H, Herrmann A, Zhang W, Zhang C, et al. S1pr1-stat3 signaling is crucial for myeloid cell colonization at future metastatic sites. Cancer Cell. 2012;21(5):642–54.
56. Liu H, Liu Y, Sun P, Leng K, Xu Y, Mei L, et al. Colorectal cancer-derived exosomal mir-106b-3p promotes metastasis by down-regulating dlc-1 expression. Clin Sci (Lond). 2020;134(4):419–34.

Publisher's note